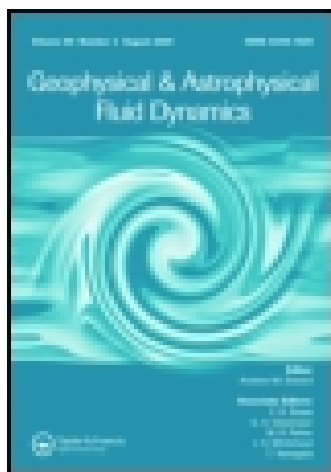


This article was downloaded by: [89.234.79.13]

On: 02 October 2014, At: 01:51

Publisher: Taylor & Francis

Informa Ltd Registered in England and Wales Registered Number: 1072954 Registered office: Mortimer House, 37-41 Mortimer Street, London W1T 3JH, UK



## Geophysical & Astrophysical Fluid Dynamics

Publication details, including instructions for authors and subscription information:

<http://www.tandfonline.com/loi/ggaf20>

### The formation of vesicular cylinders in pahoehoe lava flows

A.C. Fowler<sup>ab</sup>, Alison C. Rust<sup>c</sup> & M. Vynnycky<sup>ad</sup>

<sup>a</sup> MACSI, University of Limerick, Limerick, Ireland.

<sup>b</sup> OCIAM, University of Oxford, Oxford, UK.

<sup>c</sup> Department of Earth Sciences, University of Bristol, Bristol, UK.

<sup>d</sup> Department of Materials Science and Engineering, Royal Institute of Technology, Stockholm, Sweden.

Published online: 29 Sep 2014.



CrossMark

[Click for updates](#)

To cite this article: A.C. Fowler, Alison C. Rust & M. Vynnycky (2014): The formation of vesicular cylinders in pahoehoe lava flows, *Geophysical & Astrophysical Fluid Dynamics*, DOI: [10.1080/03091929.2014.955799](https://doi.org/10.1080/03091929.2014.955799)

To link to this article: <http://dx.doi.org/10.1080/03091929.2014.955799>

PLEASE SCROLL DOWN FOR ARTICLE

Taylor & Francis makes every effort to ensure the accuracy of all the information (the "Content") contained in the publications on our platform. However, Taylor & Francis, our agents, and our licensors make no representations or warranties whatsoever as to the accuracy, completeness, or suitability for any purpose of the Content. Any opinions and views expressed in this publication are the opinions and views of the authors, and are not the views of or endorsed by Taylor & Francis. The accuracy of the Content should not be relied upon and should be independently verified with primary sources of information. Taylor and Francis shall not be liable for any losses, actions, claims, proceedings, demands, costs, expenses, damages, and other liabilities whatsoever or howsoever caused arising directly or indirectly in connection with, in relation to or arising out of the use of the Content.

This article may be used for research, teaching, and private study purposes. Any substantial or systematic reproduction, redistribution, reselling, loan, sub-licensing, systematic supply, or distribution in any form to anyone is expressly forbidden. Terms &

Conditions of access and use can be found at <http://www.tandfonline.com/page/terms-and-conditions>

# The formation of vesicular cylinders in pahoehoe lava flows

A.C. FOWLER\*<sup>†‡</sup>, ALISON C. RUST<sup>§</sup> and M. VYNNYCKY<sup>¶¶</sup>

<sup>†</sup>MACSI, University of Limerick, Limerick, Ireland

<sup>‡</sup>OCIAM, University of Oxford, Oxford, UK

<sup>§</sup>Department of Earth Sciences, University of Bristol, Bristol, UK

<sup>¶¶</sup>Department of Materials Science and Engineering, Royal Institute of Technology, Stockholm, Sweden

*(Received 20 February 2014; in final form 14 August 2014)*

Vertical cylinders of bubble-enriched, chemically evolved volcanic rock are found in many inflated pahoehoe lava flows. We provide a putative theoretical explanation for their formation, based on a description of a crystallising three-phase (liquid, solid, gas) crystal pile in which the water-saturated silicate melt exsolves steam and becomes more silica-rich as it crystallises anhydrous minerals. These cylinders resemble pipes that form in solidifying binary alloys as a result of sufficiently vigorous porous medium convection within the mush. A convection model with the addition of gas bubbles that provide the buoyancy source indicates that the effective Rayleigh number is too low for convection to occur in the mush of a basalt lava flow. However, the formation of gas bubbles during crystallisation means that the base state includes fluid migration up through the crystal mush even without convection. Stability considerations suggest that it is plausible to form a positive feedback where increased local porosity causes increased upwards fluid flow, which brings more silicic melt up and lowers the liquidus temperature, promoting locally higher porosity. Numerical solutions show that there are steady solutions in which cylinders form, and we conclude that this model provides a viable explanation for vesicular cylinder formation in inflated basalt lava flows.

*Keywords:* Pahoehoe; Vesicular columns; Convection in lava; Three-phase flow

## 1. Introduction

Channelled flows occur in a wide variety of geophysical contexts, and in many of these, the channels are formed through the erosion by the fluid of the substrate through which it flows. Familiar examples are internal conduit flow in karstic cave systems (Groves and Howard 1994) and geysers (Dowden *et al.* 1991), both due to dissolution of host rock by groundwater. Other examples include subaerial river channels formed through the erosion of sediment by water (Smith and Bretherton 1972), subglacial channels formed through the melting of ice by water (Röthlisberger 1972) and brine channels in sea ice formed by the dissolution of ice by saline sea water (Wettlaufer *et al.* 1997) in a process analogous to the formation of freckles in alloys (Flemings 1974). It has also been suggested that similar channels form in the asthenosphere through the melting of rock by reactive flow of melt through it (Kelemen *et al.* 1997). Our concern in this paper is with the vertical features that form in pahoehoe lava flows that appear

---

\*Corresponding author. Email: [andrew.fowler@ul.ie](mailto:andrew.fowler@ul.ie)

similar to brine channels or alloy freckles, and we will advance the idea that they form in similar ways, though as we shall see, the detailed process appears more complicated than the examples mentioned above.

Pahoehoe lava flows thicken by the injection of hot magma below a cooler crust (Hon *et al.* 1994, Self *et al.* 1998). This process known as inflation is thermally efficient and is important for the development of large flood basalt flow fields as well as small flow toes. Sections through completely cooled inflated basalt flows that are now solid rocks can show a remarkable range of bubbly features including layers of vesicular (i.e. bubbly) basalt in the upper crust, horizontal sheets and vertical cylinders of vesicular evolved rock within the relatively low porosity core of the flow, and elongate bubbles called “pipe vesicles” in the lower crust. Both bubble buoyancy and expansion are thought to be important in generating these features, which are diagnostic of inflated flows. The focus of this paper is the origin of the vertical vesicular cylinders in the core of many inflated pahoehoe flows; these are usually called “vesicle cylinders” (e.g. Goff 1996), but “vesicular cylinders” is more apt as they consist of melt with numerous bubbles, and this term is clearly distinct from “pipe vesicle”, which refers to a single elongate bubble near the base of a pahoehoe lava flow. There are also much rarer vertical cylindrical features in non-inflated basalt lava with vesicularity and chemistry distinct from vesicular cylinders that Kontak and Dostal (2010) term “segregation pipes”; these seem to have a different origin and are not considered here.

The upper and lower crusts of outcrops of solidified inflated lava flows are recognised by their higher vesicularity (i.e. greater bubble content) and lower crystallinity (i.e. greater glass content) than the core of the flow. The final thickness of the upper crust is almost always 40–60% of the lava flow and has been directly related to the duration of inflation (Hon *et al.* 1994), whereas the lower crust is 20–100 cm thick regardless of the overall lava flow thickness (Self *et al.* 1998). The paradigm is that the very top and bottom of the lava cool quickly enough that bubbles are quenched in place but bubbles rise easily through the hot interior and collect below the upper crust. As the upper crust continues to cool and thicken, it preserves layers of vesicular basalt. Each of these bubbly layers is thought to correspond to a pulse of pressure change and/or injection of fresh magma that introduced new bubbles into the lava (Hon *et al.* 1994, Cashman and Kauahikaua 1997). The rise of bubbles leaves a non-vesicular core. However, as the base cools and crystallises, incompatible elements including water concentrate in the residual silicate melt, and new bubbles form in the mush making the interstitial fluid (melt and bubbles) buoyant. Obstructed by crystals, the bubbles do not rise freely; rather their growth causes segregation by pushing residual melt and bubbles out between the crystals (Anderson *et al.* 1984). The bubbly residuum somehow rises through the lava in vertical cylinders and then seems to spread laterally into vesicular sheets.

In a given lava flow, the diameter of the vesicular cylinders and the spacing between them are fairly constant, typically centimetres in diameter and tens of centimetres (e.g. figure 1) to a metre apart. The cylinders often begin within 0.25 m of the lava flow base and can be up to several meters in height (Goff 1996). The vesicularity (i.e. gas volume fraction) of the cylinders is typically 10–30% (Goff 1996, Rogan *et al.* 1996), which is about 2–5 times greater than the vesicularity of the basalt that hosts them (Rogan *et al.* 1996). In the flows studied by Rogan *et al.* (1996), Stephenson *et al.* (2000), Hartley and Thardarson (2009) and Sigmarsson *et al.* (2009), the chemical composition of the segregated material which makes up the vesicular cylinders corresponds to the residual melt from 36–50%, 43–47%, 30–40% and 50–60% crystallisation of the host basalt, respectively. The boundaries between the host basalt and the more silicic vesicular cylinders and sheets are sharp, in contrast to the gradational boundaries of the vesicular basalt layers in the upper crust.



Figure 1. Vesicular cylinders at Blackhead on the Antrim coast, Northern Ireland. The upper picture shows the vertical cylinders, as marked with arrows. Although there is clearly some jointing (fractures in rock), most of the dark vertical stripes represent bubble-rich flow pipes. The lower picture shows a sub-horizontal transverse section. Numerous cylinder cross-sections are visible as round pits at the surface due to preferential weathering of the vesicular rock in the cylinders compared to the host rock.

Several researchers have considered the origins of vesicular cylinders. [Goff \(1977\)](#) proposed that bubbly residual fluid collects on the top of mush near the bottom of the flow and that the vesicular cylinders develop from this layer of buoyant fluid because of Rayleigh–Taylor instabilities. [Goff \(1996\)](#) later dismissed Rayleigh–Taylor instabilities citing issues with the fluid viscosities and the lack of field evidence that a suitable bubbly layer once existed in the flow. [Manga and Stone \(1994\)](#) suggested that cylinders develop from instabilities of bubble concentration; however, this model is inconsistent with the fact that the cylinders comprise liquid of more evolved (i.e. more silicic) chemical composition than the magma that surrounds them. Others (e.g. [Caroff \*et al.\* 2000](#)) considered vesicular cylinders to be solidified elongated diapirs, but did not focus on diapir formation itself. [Costa \*et al.\* \(2006\)](#) returned to the Rayleigh–Taylor instability model. Based on the spacing of cylinders and theory of [Lister and Kerr \(1989\)](#), they found that a layer of bubbly residuum accumulating on top of the lower mush became unstable when about 2 cm thick. If the instabilities grew up into a liquid lava flow core, then inflation would have had to have ceased; otherwise lateral magma flow would have disturbed the vertical path of the rising finger of vesicular melt. Furthermore, to preserve cylinders generated by Rayleigh–Taylor instabilities, the growing lower mush would have to

keep supplying segregated bubbly fluid at a rate sufficient to prevent blobs of bubbly fluid from detaching.

Recent work has included case studies of specific inflated lava flows, constraining qualitative models of cylinder formation from geological field observations, petrology and chemistry. In separate studies of the Levering lava flow, USA, and Surtsey lavas, Iceland, [Hartley and Thardarson \(2009\)](#) and [Sigmarsson \*et al.\* \(2009\)](#) conclude that the segregated material in the vesicular cylinders (and vesicular sheets) originated from mush near the base of the flow; [Hartley and Thardarson \(2009\)](#) emphasise that the vesicular cylinders in the Levering flow were fed by pipe vesicles preserved in the lower crust. In contrast, in a study of the Kutsugata lava flow in Japan, [Kuritani \*et al.\* \(2010\)](#) propose that the head of the growing vesicular cylinder was fed laterally by flow of residuum from the nearby host lava into the cylinder. Also in contrast to previous studies of other lava flows, [Kuritani \*et al.\* \(2010\)](#) conclude that the vesicular cylinders and the vesicular sheets above them in the Kutsugata lava flow are not genetically related. Vesicular cylinders and other segregation features in basalt lava flows have continued to attract attention both because they are common features and because understanding their origin may provide insights into the role of vesiculation in driving magma segregation in other contexts that are less accessible to field study than lava flow deposits. However, physical interpretations of their origin are still largely conceptual.

An alternative explanation for vesicular cylinders that we consider here is so called “mushy convection” ([Worster 1997](#)). In essence, flow within a stationary crystallising mush is driven by gradients in liquid density that are generated because some components are preferentially incorporated into the crystals leaving a buoyant residual liquid. Because crystallisation is incongruent, flow of liquid through the crystal pile locally changes the bulk (liquid+crystal) composition, and thus changes the liquidus temperature leading to changes in the volume fraction of crystals and the permeability of the mush. One possible consequence of natural convection in mushy layers is the focussing of the flow to produce “chimneys” which are narrow, vertical channels devoid of crystals. These chimneys are observed in solidifying aqueous salt solutions ([Tait \*et al.\* 1992](#)), sea ice mushes and castings of metallic alloys ([Worster 1997](#)). It has been suggested that mushy convection could occur in the Earth’s core and could explain chimney structures in the Bushveld ultramafic complex ([Tait and Jaupart 1992](#)). However, mushy convection does not seem to have attracted attention in the basalt lava flow literature. A significant difference between classic mushy convection and the lava flow application is that in the latter, the growth of steam bubbles as the mush crystallises induces pore fluid flow up through the permeable crystal pile even if there is no convective instability. This bubble growth-driven upward flow suggests another potential explanation for vesicular cylinders: unidirectional flow can lead to channelisation if there is a suitable feedback between velocity and permeability, analogous to the formation of melt channels in the mantle (e.g. [Hewitt and Fowler 2009](#)).

It is not tractable to include a complete phase diagram for the magma in theoretical models of mushy convection and melt channelisation. As a molten basalt cools, it forms various crystals such as olivine, plagioclase and pyroxene, each of which is a solid solution with changes in their chemistry as crystallisation of the magma proceeds. Basalt is about 50 weight % silica ( $\text{SiO}_2$ ) and the residual melt becomes more silicic (along with other chemical changes) as the basalt crystallises. Here, we consider migration and re-equilibration of the melt (and suspended steam bubbles) through the porous crystal pile which means that the local bulk composition will vary spatially, and a phase diagram for a bulk composition of basalt is insufficient to model these processes. We, therefore, employ a highly simplified phase diagram (figure 2) as

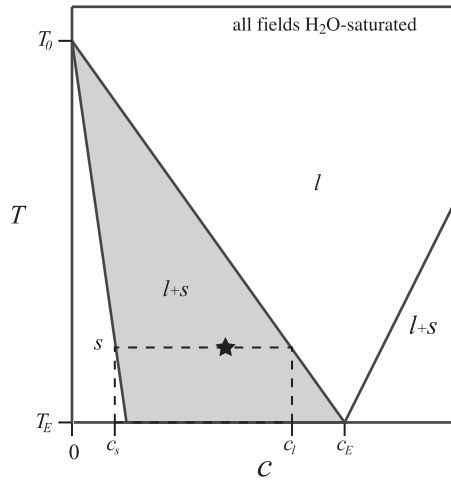


Figure 2. Diagram showing what phases exist for a bulk composition  $c$  and temperature  $T$ , where  $s$  refers to solid crystals and  $l$  to liquid silicate melt. The system is water saturated, and so there are also steam bubbles present in all fields. The average composition of the modelled mush is in the shaded region which is bounded above by the liquidus, which is the line from  $(0, T_0)$  to the eutectic at  $(c_E, T_E)$ . For the point marked with a star, the crystal composition,  $c_s$ , and the liquid composition,  $c_l$ , are indicated as an example.

described below to assess the feasibility of generating vesicular cylinders in basalt lava flows by mushy convection and melt channelisation.

## 2. Convection in a crystal pile

In the model which we now describe, a good deal of nomenclature arises, and a listing of all this is given in the appendix. We consider a crystal pile, as shown in figure 3, with porosity  $\phi$ , containing a pore fluid composed of liquid silicate melt and exsolved bubbles of water vapour. The relative (to the porosity) volume fraction of the gas is denoted as  $\alpha$  and so the bulk vesicularity is  $\alpha\phi$ . For simplicity, we suppose that, in addition to water which is always present as steam bubbles and dissolved in the silicate liquid melt, the magma is composed of two anhydrous components. One has an abundance (measured as volume fraction of liquid) of  $c$  and the other  $1 - c$ , where  $0 \leq c \leq 1$ . Although not entirely geologically accurate, we refer to  $c$  as the silica composition of the magma with the silica composition of the liquid being  $c_l$ , and that of the solid crystals being  $c_s$ ; as the magma cools and crystallises  $c_l$  increases as does the true silica content of the melt. The dissolved water concentration is denoted  $c_{\text{H}_2\text{O}}$ , and is assumed constant (at saturation). The Darcy flux through the crystal pile is denoted by  $\mathbf{u}$ , and the pressure in the liquid phase is denoted as  $p$ . The model below assumes that the pore liquid and gas move homogeneously through the pore space, and also that the pressure in the liquid and gas phases is equal. While there is a pressure difference due to surface tension, this is not relevant since the bubbles are isolated.

The equations we propose to describe convection within the mush are the following. Conservation of the solid phase takes the form

$$-\rho_s \phi_t = m_c, \quad (1)$$

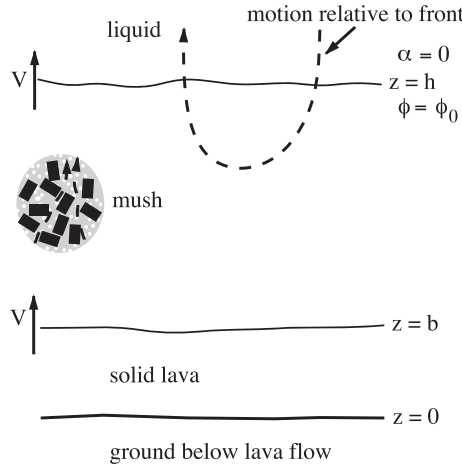


Figure 3. Illustration of the model set-up. The crystal pile is bounded above by its upper mush–liquid interface  $z = h$ , whose location is determined by a Stefan condition, as is also the lower mush–solid boundary  $z = b$ . In our model, we assume thermal conditions are such that both fronts move at speed  $V$ . The mush acts as a porous medium of porosity  $\phi$  and pore volume gas fraction  $\alpha$ , and these are prescribed at the upper surface (as  $\phi_0$  and 0, respectively), *providing the lava above is being sucked into the moving upper interface*, see (20) and (21). When circulation occurs such that there is net expulsion of gas-rich lava from the mush, the prescription of  $\alpha = 0$  is no longer possible.

where here and henceforward the subscript  $t$  denotes partial differentiation with respect to time,  $\rho_s$  is the crystal density and  $m_c$  is the rate of crystallisation (with units of mass per unit volume per unit time). The pore fluid density is given by

$$\rho = \rho_l(1 - \alpha) + \rho_g\alpha, \quad (2)$$

where  $\rho_l$  is the melt (liquid) density and  $\rho_g$  is the exsolved gas density, assumed here to be  $\text{H}_2\text{O}$ . All three densities are assumed to be constant, since their variation with composition and temperature is dwarfed by that in (2) due to variation in  $\alpha$ . Conservation of mass of the pore fluid then yields the equation

$$(\rho\phi)_t + \nabla \cdot (\rho\mathbf{u}) = -m_c, \quad (3)$$

and we suppose that the fluid flux  $\mathbf{u}$  through the crystal pile is determined by Darcy's law in the form

$$\mathbf{u} = -\frac{K}{\eta_l}(\nabla p + \rho g \hat{\mathbf{k}}), \quad (4)$$

where  $g$  is the acceleration due to gravity,  $K$  is the permeability of the crystal pile,  $\eta_l$  is the viscosity of the melt and  $\hat{\mathbf{k}}$  is the unit vector in the vertical direction.

Conservation of the dissolved water phase is determined by

$$(\rho_l(1 - \alpha)\phi c_{\text{H}_2\text{O}})_t + \nabla \cdot [(\rho_l(1 - \alpha)c_{\text{H}_2\text{O}})\mathbf{u}] = -m_v, \quad (5)$$

while conservation of the gaseous water phase is given by

$$(\rho_g\alpha\phi)_t + \nabla \cdot (\rho_g\alpha\mathbf{u}) = m_v, \quad (6)$$

with  $m_v$  being the rate of exsolution.

Conservation of the liquid silica concentration  $c_l$  is given by

$$(\rho_l(1 - \alpha)\phi c_l)_t + \nabla \cdot (\rho_l(1 - \alpha)c_l\mathbf{u}) = -m_s, \quad (7)$$

while that of the solid silica concentration  $c_s$  is

$$(\rho_s(1 - \phi)c_s)_t = m_s, \quad (8)$$

where  $m_s$  is the surface source term.

The energy equation can be written in the form

$$\begin{aligned} (\rho_s(1 - \phi)c_{ps} + \rho c_p \phi)T_t + \rho c_p \mathbf{u} \cdot \nabla T - (p_t + \mathbf{u} \cdot \nabla p) \\ = k_T \nabla^2 T + L_c m_c + L_v m_v, \end{aligned} \quad (9)$$

where

$$\begin{aligned} \rho c_p &= \rho_l(1 - \alpha)c_{pl} + \rho_g \alpha c_{pg}, \\ k_T &= \phi(1 - \alpha)k_l + \phi \alpha k_g + (1 - \phi)k_s, \end{aligned} \quad (10)$$

$c_{ps}$ ,  $c_{pl}$  and  $c_{pg}$  are the specific heats of solid, liquid and gas, respectively, and  $k_s$ ,  $k_l$  and  $k_g$  are the corresponding thermal conductivities;  $L_c$  and  $L_v$  are the latent heats of crystallisation and exsolution, respectively.

Finally, the temperature  $T$  is constrained to lie on the liquidus, which we take to depend linearly on silica composition, thus

$$T = T_L(c_l) = T_0 - m_L c_l, \quad (11)$$

and the solid composition is taken to lie on the solidus, again supposed linear, thus

$$c_s = \Lambda c_l, \quad (12)$$

where  $0 \leq \Lambda < 1$  is the partition coefficient, i.e. the ratio of solidus to liquidus concentrations.† The surface source term in (8) is related to the rate of crystallisation by

$$m_s = m_c \Lambda c_l. \quad (13)$$

The principal variables of the model are  $\phi$ ,  $\alpha$ ,  $\mathbf{u}$ ,  $p$ ,  $c_l$  and  $c_s$ , and these are described by the equations (1), (5), (4), (3), (7) and (8). The energy equation (10) determines the crystallisation rate  $m_c$ , (6) determines the exsolution rate,  $m_v$ , and  $T$  and  $c_s$  are given by (11) and (12). The model is thus closed, when sufficient boundary conditions are given. These are discussed later.

## 2.1. Non-dimensionalisation

For simplicity, we suppose all the specific heats  $c_{ps} = c_{pl} = c_{pg} = c_p$  and thermal conductivities  $k_s = k_l = k_g = k_T$  are the same. The most disparate of these is the thermal conductivity of steam in the bubbles,  $k_g$ , which is substantially smaller than  $k_s$  and  $k_l$ . Considering the geological evidence suggests  $\phi \alpha < 0.3$  (section 1), then  $k_T$  could be up to about 30% less than the assumed  $k_T$  (10). The resulting overestimate in heat transfer by thermal conduction through the bubbly magma is partially offset by heat transfer across the steam bubbles by radiation and vapour convection that are not included.

†Strictly (12) only applies at the crystal interface. For conditions of slow crystallisation, it can be shown to apply generally.

We non-dimensionalise the model by scaling the variables as follows:

$$\begin{aligned} t &\sim \frac{d^2}{\kappa_T}, & |\mathbf{u}| &\sim \frac{\kappa_T}{d}, & |\mathbf{x}| &\sim d, & m_c &\sim \frac{k_T m_L}{L_c d^2}, \\ \rho &\sim \rho_l, & m_v &\sim \frac{\rho_g \kappa_T}{d^2}, & p + \rho_l g z &\sim \frac{\eta_l \kappa_T}{K_0}, \end{aligned} \quad (14)$$

where  $d$  is the magma depth,

$$\kappa_T = \frac{k_T}{\rho_l c_p}, \quad (15)$$

is the thermal diffusivity and we write the permeability in the form

$$K = K_0 \Pi(\phi); \quad (16)$$

the resulting dimensionless model takes the form, where we now also write  $c_l = c$ ,

$$\begin{aligned} \rho &= 1 - \alpha + \delta \alpha, & \mathbf{u} &= -\Pi(\phi) \nabla p + R(1 - \delta) \alpha \hat{\mathbf{k}}, \\ -(1+r)St \phi_t &= m_c, & St[(\rho\phi)_t + \nabla \cdot (\rho\mathbf{u})] &= -m_c, \\ (\phi\alpha)_t + \nabla \cdot (\alpha\mathbf{u}) &= m_v, & \sigma[((1-\alpha)\phi)_t + \nabla \cdot ((1-\alpha)\mathbf{u})] &= -m_v, \\ St[(1+r)(1-\phi)c_s]_t &= \Lambda c, & St[((1-\alpha)\phi c)_t + \nabla \cdot ((1-\alpha)c\mathbf{u})] &= -\Lambda c, \\ [(1+r)(1-\phi) + \rho\phi]c_t + \rho\mathbf{u} \cdot \nabla c + \frac{\beta}{R} \left( \frac{\partial}{\partial t} + \mathbf{u} \cdot \nabla \right) (p - Rz) & & & \\ & & & = \nabla^2 c - m_c - \delta S_v m_v. \end{aligned} \quad (17)$$

The dimensionless parameters are defined by

$$\begin{aligned} r &= \frac{\rho_s - \rho_l}{\rho_l}, & \delta &= \frac{\rho_g}{\rho_l}, & St &= \frac{L_c}{m_L c_p}, \\ R &= \frac{\rho_l g d K_0}{\eta_l \kappa_T}, & \sigma &= \frac{\rho_l c_{\text{H}_2\text{O}}}{\rho_g}, & \beta &= \frac{g d}{m_L c_p}, & S_v &= \frac{L_v}{m_L c_p}. \end{aligned} \quad (18)$$

Table 1. Assumed values of constants. It is assumed that the specific heats and thermal conductivities of gas, liquid and solid are the same.

Symbol	Meaning	Typical value
$c_{\text{H}_2\text{O}}$	Water saturation	$10^{-3}$
$c_p$	Specific heat	$10^3 \text{ J kg}^{-1} \text{ K}^{-1}$
$d$	Magma depth	1 m
$g$	Gravity	$9.8 \text{ m s}^{-2}$
$K_0$	Permeability scale	$2 \times 10^{-10} \text{ m}^2$
$k_T$	Thermal conductivity	$= \rho_l c_p \kappa_T$
$L_c$	Latent heat of crystallisation	$3 \times 10^5 \text{ J kg}^{-1}$
$L_v$	Latent heat of exsolution	$3 \times 10^5 \text{ J kg}^{-1}$
$m_L$	Liquidus slope	100 K
$\kappa_T$	Thermal diffusivity	$0.7 \times 10^{-6} \text{ m}^2 \text{ s}^{-1}$
$\eta_l$	Melt viscosity	$10^2 \text{ Pa s}$
$\Lambda$	Partition coefficient	0.2
$\rho_s$	Crystal density	$2.7 \times 10^3 \text{ kg m}^{-3}$
$\rho_l$	Melt density	$2.6 \times 10^3 \text{ kg m}^{-3}$
$\rho_g$	Water vapour density	$1 \text{ kg m}^{-3}$

Table 2. Typical values of parameters.

Parameter	Typical value	Interpretation
$r$	0.04	Solid–liquid density difference
$R$	0.15	Effective Rayleigh number
$St$	3	Stefan number
$S_v$	3	Vapour Stefan number
$\beta$	$10^{-4}$	Adiabatic heating
$\delta$	$0.4 \times 10^{-3}$	Gas–liquid density ratio
$\sigma$	2.7	Dissolved to exsolved vapour density ratio

Using the parameter values in table 1, we calculate typical values of these parameters as shown in table 2.

## 2.2. A reduced model

From table 2, we see that  $r$ ,  $\beta$  and  $\delta$  are all small. Putting these to zero, the model can be reduced, after some manipulation, to the form

$$\begin{aligned}
 \nabla \cdot \mathbf{u} &= (\phi\alpha)_t + \nabla \cdot (\alpha\mathbf{u}) = -\sigma\phi_t, \\
 \mathbf{u} &= -\Pi(\phi)\nabla p + R\alpha\hat{\mathbf{k}}, \\
 St[(1-\alpha)(\phi c_t + \mathbf{u} \cdot \nabla c) + c\phi_t] &= -\Lambda c, \\
 (1-\alpha\phi)c_t + (1-\alpha)\mathbf{u} \cdot \nabla c &= \nabla^2 c + St\phi_t.
 \end{aligned} \tag{19}$$

In addition, we will suppose that  $\Lambda = 0$ , as is the case in aqueous solutions.

The parameter  $R$  plays the rôle in (19) of a Rayleigh number for porous medium convection, and we shall, henceforth, refer to it as an effective Rayleigh number. Indeed, (19) appears to generalise the Boussinesq equations of porous medium convection (to whose form they reduce if we take  $\sigma = 0$ ,  $\Pi = 1$ ,  $\phi$  and  $\alpha$  constant, and ignore the third equation via  $St = \Lambda = 0$ ), but no genuine simple parametric reduction to them is available.

## 2.3. Boundary conditions

At the upper surface of the crystal mush, we suppose that the crystal fraction is specified,

$$\phi = \phi_0 \quad \text{at} \quad z = h, \tag{20}$$

this defining where the essentially solid crystal mush undergoes the transition to a crystal-rich fluid. We also suppose that the magma above the mush is bubble-free, thus

$$\alpha = 0 \quad \text{if} \quad u_n - \phi V_n < 0 \quad \text{at} \quad z = h, \tag{21}$$

where  $V_n$  is the normal component of the surface velocity and  $u_n$  is the normal component of the Darcy flux. This condition ensures liquid inflow to the mush; if it is not satisfied,  $\alpha$  cannot be prescribed, and indeed this is also the condition for channel formation (see below).

To be more specific, we conceive of the magma above the mush as a viscous fluid, cooled from above and below. Calculation of an appropriate Rayleigh number for this fluid indicates that thermal convection will be vigorous, but since the fluid layer is cooled from above and

below, convection will be of the box-filling type; that is to say, dense plumes of fluid will descend towards the lower unit, where they will pond, and deliver a conductive heat flux to the underlying mush, which will decrease as the ponded layer thickens and the magma cools. It is, therefore, appropriate to specify a conductive heat flux above the mush, and in dimensionless terms, this can be written as

$$\mathbf{n} \cdot \nabla c = -\gamma_+ \quad \text{at } z = h, \quad (22)$$

where  $\mathbf{n}$  is the normal directed away from the mush.

The final two conditions at the surface are those of constant pressure, and an assumed prescribed temperature at the base of the fluid, which implies a known silica concentration; thus

$$p = 0, \quad c = c_0 \quad \text{at } z = h. \quad (23)$$

At the lower surface, which we take to be  $z = b$ , we form a flow boundary condition from a pill-box argument on the mass conservation equations. There are three of these: the sums of (1) and (3), (5) and (6) and (7) and (8). The second pair serves to determine the retained water in the solidified lava, the third pair serves to determine the ‘‘silica’’ composition of the solid (since we suppose the solid/mush interface is at the eutectic) and the first pair yields a flow boundary condition for the pore fluid, which takes the dimensionless form

$$u_n = -\phi V_n \left[ \frac{r + (1 - \delta)\alpha}{1 - (1 - \delta)\alpha} \right] \quad \text{at } z = b. \quad (24)$$

In conditions where the lower boundary is slowly moving (Worster 1986), or if  $r$  and  $\alpha$  are small, the fluid flow is small, and for simplicity, we will take it to be zero. Additionally, the temperature is supposed to be at the eutectic point, thus the concentration is also eutectic: hence

$$u_n = 0, \quad c = c_E \quad \text{at } z = b. \quad (25)$$

Generally, the lower boundary  $b$  of the mush is not known, and will be determined by a Stefan condition describing the freezing of the mush to a completely solid phase; analogously to (22), we write

$$\mathbf{n} \cdot \nabla c = -\gamma_- \quad \text{at } z = b. \quad (26)$$

## 2.4. Basic channel formation mechanism

The model we have described is very familiar in metallurgy, where the solidification of alloys has been studied for a long time (Flemings 1974). It is well known in the casting of alloys that crystallisation normally occurs through the formation of a mushy layer of mixed crystals and liquid between the already crystallised solid and the liquid. Convection of the liquid through the porous mush typically occurs and if this convection is sufficiently vigorous, then channels form, and these are visible in the final casting as spots, usually called freckles.

The formation of freckles is associated with the following kinematic explanation, which we illustrate for the case that the partition coefficient  $\Lambda$  is zero. At the upper crystal surface  $z = h$ , we prescribe  $\phi = \phi_0$ , and require that  $\phi_t < 0$  in order that crystallisation proceed. If this is not the case, then redissolution occurs, which is inconsistent with the advance of the crystallisation front. Therefore, we suppose that channels will form when

$$\phi_t \Big|_{z=h} > 0. \quad (27)$$

From (19)<sub>3</sub> (with  $\Lambda = 0$ ), this is the case if and only if

$$\phi c_t + \mathbf{u} \cdot \nabla c < 0 \quad \text{at} \quad z = h. \quad (28)$$

However,  $c \equiv c_0$  at  $z = h$ , and thus

$$c_t + \mathbf{V} \cdot \nabla c = 0 \quad \text{at} \quad z = h, \quad (29)$$

where  $\mathbf{V}$  is the velocity of the upper crystal surface. Since the normal derivative  $\mathbf{n} \cdot \nabla c < 0$ , we see that the criterion (27) for channel formation is equivalent to

$$u_n|_{z=h} > \phi V_n, \quad (30)$$

that is to say, the pore fluid velocity (not flux) is larger than the front advance speed.

In alloy solidification, the pore fluid velocity is caused by compositional convection. The distinction in the present case is that the fluid velocity is induced by the exsolution of steam, which is manifested in the model through the non-zero value of  $\sigma$ , which induces a pore fluid flow out of the crystal mush.

## 2.5. One-dimensional model

In one space dimension, the mush occupies the region  $b(t) < z < h(t)$ , the pore pressure is uncoupled and the model (19) reduces (with  $\Lambda = 0$ ) to the form

$$\begin{aligned} w_z &= -\sigma \phi_t = (\phi \alpha)_t + (\alpha w)_z, \\ (1 - \alpha)(\phi c_t + w c_z) + c \phi_t &= 0, \\ (1 - \alpha \phi) c_t + (1 - \alpha) w c_z &= c_{zz} + St \phi_t, \end{aligned} \quad (31)$$

where the subscript  $z$  denotes partial differentiation with respect to  $z$  (and the subscript  $t$  is still a time derivative), together with the boundary conditions

$$\begin{aligned} \alpha = 0, \quad \phi = \phi_0, \quad c = c_0 \quad &\text{on} \quad z = h, \\ w = 0, \quad c = c_E \quad &\text{on} \quad z = b. \end{aligned} \quad (32)$$

Determination of the upper and lower surfaces is effected through the flux conditions

$$\begin{aligned} c_z &= -\gamma_+ \quad \text{on} \quad z = h, \\ c_z &= -\gamma_- \quad \text{on} \quad z = b. \end{aligned} \quad (33)$$

where, as we shall see, we would then require  $\gamma_- > \gamma_+$ .

## 2.6. Travelling wave solution

After a long time, we might expect the solution of (31) and (32) to tend to a travelling wave solution, at least if the boundary fluxes  $\gamma_{\pm}$  are constant. We, therefore, seek a solution in which the variables are functions of

$$\xi = h - z, \quad h = Vt, \quad b = Vt - \xi_b, \quad (34)$$

so that  $w$ ,  $\phi$ ,  $\alpha$  and  $c$  satisfy the equations

$$\begin{aligned} -w' &= -\sigma V \phi' = V(\phi \alpha)' - (\alpha w)', \\ (1 - \alpha)(V \phi c' - w c') + V c \phi' &= 0, \\ (1 - \alpha \phi) V c' - (1 - \alpha) w c' &= c'' + St V \phi', \end{aligned} \quad (35)$$

where the primes denote differentiation with respect to  $\xi$ , together with the boundary conditions

$$\begin{aligned} \alpha = 0, \quad \phi = \phi_0, \quad c = c_0, \quad c' = \gamma_+ \quad & \text{on } \xi = 0, \\ w = 0, \quad c = c_E, \quad c' = \gamma_- \quad & \text{on } \xi = \xi_b. \end{aligned} \quad (36)$$

The model is of fourth order, and the extra flux boundary conditions must be used to determine the unknown propagation speed  $V$  and depth  $\xi_b$ .

The equations (35) permit four first integrals. We can use three of these to find expressions for  $w$ ,  $\alpha$  and  $\phi$  in terms of  $c$ , and after some manipulations, the solutions can be written in the following form. It is convenient to define

$$X(c) = c/c_0 \geq 1, \quad (37)$$

together with its value at the base,

$$X_E = c_E/c_0. \quad (38)$$

We then have

$$w = \sigma V(\phi - \phi_b), \quad \alpha = \frac{\sigma(\phi_0 - \phi)}{(1 - \sigma)\phi + \sigma\phi_b}, \quad \phi = \frac{\phi_0 + \sigma(1 - X)(\phi_b - \phi_0)}{X}, \quad (39)$$

where the basal porosity is

$$\phi_b = \frac{\phi_0[\sigma X_E + (1 - \sigma)]}{(1 + \sigma)X_E - \sigma}. \quad (40)$$

$\phi$  is a monotonically decreasing function of  $c$ . Eliminating  $\phi_b$  from these expressions, we find

$$\phi = \frac{\phi_0[X_E + \sigma(X_E - 1)X]}{X[X_E + \sigma(X_E - 1)]}, \quad w = \frac{\sigma V\phi_0(X_E - X)}{X[X_E + \sigma(X_E - 1)]}, \quad \alpha = \frac{\sigma(X - 1)}{1 + \sigma(X - 1)}. \quad (41)$$

It is easy to see that

$$\frac{w|_{\xi=0}}{\phi_0 V} = \frac{\sigma(X_E - 1)}{X_E + \sigma(X_E - 1)} < 1, \quad (42)$$

and thus the channel-forming criterion (30) is never satisfied. This suggests that, if (30) is indeed the correct criterion for channel formation, some form of instability must occur. This is discussed further later.

The solution is completed by solving the first-order equation for  $c$  which follows from the last of the first integrals constructed from (35), and with some algebra, can be written in the form

$$c' = Vf(c) + \gamma_+, \quad (43)$$

where

$$f(c) = (1 - \phi_0)(c - c_0) + (St + c)[\phi_0 - \phi(c)]. \quad (44)$$

We solve this with the initial condition  $c = c_0$  at  $\xi = 0$ , where the wave speed is determined by

$$V = \frac{\gamma_- - \gamma_+}{f(c_E)}, \quad (45)$$

and the depth  $\xi_b$  follows from the quadrature

$$\xi_b = \int_{c_0}^{c_E} \frac{dc}{\gamma_+ + Vf(c)}. \quad (46)$$

Assuming  $\gamma_- > \gamma_+$ , then  $V$  is positive;  $f$  is a positive convex function, so that  $c$  increases monotonically with depth  $\xi$ , and  $\phi$  decreases monotonically with depth.

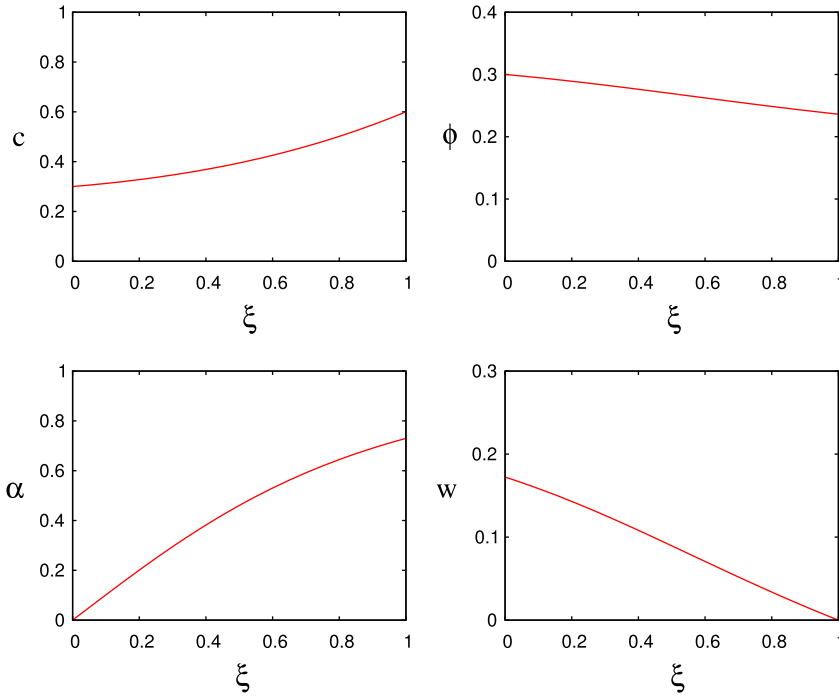


Figure 4. Solution of (43) for  $c$ , using parameter values  $\gamma_+ \approx 0.113$ ,  $V = 1$ ,  $\phi_0 = 0.3$ ,  $St = 3$ ,  $\sigma = 2.7$ ,  $c_0 = 0.3$ ,  $c_E = 0.6$  and corresponding plots of  $\phi$ ,  $\alpha$  and  $w$  as given in (41). Note that  $\xi$  is dimensionless depth below the mush–liquid interface. The value of  $\gamma_+$  is adaptively chosen in order to obtain  $c = c_E$  at  $\xi = 1$ .

Note that this solution can equally be obtained by prescribing  $V$  and  $\xi_b$ .  $\gamma_-$  is then determined via

$$\gamma_- = \gamma_+ + Vf(c_E), \quad (47)$$

and  $\gamma_+$  is determined by

$$\xi_b = \int_{c_0}^{c_E} \frac{dc}{\gamma_+ + Vf(c)}. \quad (48)$$

One can choose  $V = \xi_b = 1$  without loss of generality. To see this, note that the integral in (48) decreases monotonically as a function of  $\gamma_+$ , and the integral is (logarithmically) infinite at  $c = c_0$ , hence there is a (unique) solution for  $\gamma_+$ . For numerical purposes, it is convenient to solve the time-dependent problem in a frame moving at speed  $V = 1$ , with a fixed domain  $0 < \xi < 1$ , and ignore the flux boundary conditions, although it is also easy to use a numerical shooting method by adjusting  $\gamma_+$ . Figure 4 shows the profiles for  $c$ ,  $\phi$ ,  $\alpha$  and  $w$  obtained in this way.

### 3. Instability

There are two types of instability which seem possible. The first is convective instability, based on a sufficiently high value of the effective Rayleigh number for porous medium convection in the mush. In this view, which is analogous to what happens in alloy solidification

(Worster 1997), compositional convection is initiated at supercritical values of the effective Rayleigh number, and as  $R$  increases, the pore velocity increases, and at some point, the criterion (30) will be passed, and channels are initialised, analogously to the chimneys found in crystallising ammonium chloride solution. While this is an attractive possibility, the estimated value in table 2 is about two orders of magnitude less than that necessary for ordinary convection in an open porous medium (with conductive boundaries: impermeable below and liquid above), which is about 27 (Lapwood 1948).

The greatest uncertainty in the calculation of this effective Rayleigh number is the mush permeability at the relevant porosities ( $\phi > 0.3$ ). There is one experimental datum from Philpotts and Carroll (1996) who measured  $K = 3 \times 10^{-10} \text{ m}^2$  for a partially molten basalt lava flow sample with  $\phi = 0.66$ . We expect the relevant  $K$  will be smaller because the chemical composition of vesicular cylinders corresponds to the residual melt of the host lava that has crystallised to a lower  $\phi$  (section 1). To constrain permeability of basalt for  $0.3 < \phi < 0.8$ , Hersum *et al.* (2005) determined permeability of natural and simulated partially molten basalt microstructures (the former determined by X-ray computed tomography of natural basalt) and concluded that the porosity–permeability relationship can be described by Rumpf–Gupte or Carman–Kozeny relations. For the Carman–Kozeny relation,  $K_0 = D^2/180$ , where  $D$  is the mean length of crystals in meters. Consequently, to increase the effective Rayleigh number sufficiently for convective instability by increasing  $K_0$  to order  $10^{-8} \text{ m}^2$  requires  $D \gtrsim 1 \text{ mm}$ , which is considerably greater than  $D$  for the groundmass of basalts that host vesicular cylinders (e.g. Kuritani *et al.* 2010). Although there may be exceptional circumstances where the crystal sizes and shapes mean that the lava permeability is order  $10^{-8} \text{ m}^2$  at the crystallinity for which the mush has sufficient strength to act as a porous medium, the onset of convection prior to channel formation is unlikely, and does not seem to be a general explanation for vesicular cylinders.

An alternate mechanism of direct instability finds its analogue in the processes of stream formation and melt channel formation in the Earth’s asthenospheric mantle. Each of these situations allows direct channel formation from a unidirectional flow without the necessity to have a prior convective instability. Melt is transported slowly upwards in the asthenosphere by liquid buoyancy. One mechanism for channel formation lies in the positive feedback afforded by the following sequence (Hewitt and Fowler 2009): a local increase of melt velocity leads to a raised temperature (because the temperature is on the Clapeyron curve) which causes melting, and thus increased permeability, and thus further increase of the velocity. A similar feedback leads to rill formation in overland flow (Smith and Bretherton 1972, Fowler *et al.* 2007). A locally increased flow depth causes increased flow rate, which causes increased erosion, and thus further increase in flow depth as the soil surface is lowered. In this case, the instability mechanism is through the occurrence of a negative diffusion coefficient, whose consequent ill-posedness is regularised by the small mismatch between water surface slope and soil surface slope (Loewenherz 1991, Loewenherz-Lawrence 1994); for further detail on both these models, see Fowler (2011).

The putative way this instability would be heralded in the set of equations making up the reduced model (19) is as follows: a local increase in fluid velocity in the lava mush allows for upwards flux of higher concentration  $c$  from below. The higher concentration lowers the liquidus temperature, thus allowing dissolution of crystals and hence higher permeability, which promotes higher velocity. This seems identical to the proposed mechanism for asthenosphere magma channels, which does indeed produce channels in that case.

Based on the description above, we suppose a travelling mush with dimensionless speed  $V$  and dimensionless depth one, and we write the governing equations (19) in the form

$$\begin{aligned} \nabla \cdot \mathbf{u} &= \sigma (V\phi_Z - \phi_t), \\ (\phi\alpha)_t - V(\phi\alpha)_Z &= \nabla \cdot ((1-\alpha)\mathbf{u}), \\ \mathbf{u} &= -\Pi(\phi)\nabla p, \\ (1-\alpha)(\phi c_t - V\phi c_Z + \mathbf{u} \cdot \nabla c) + c(\phi_t - V\phi_Z) &= 0, \\ (1-\phi)(c_t - Vc_Z) &= \nabla^2 c + (c + St)(\phi_t - V\phi_Z), \end{aligned} \quad (49)$$

where the travelling wave coordinate is

$$Z = z - Vt, \quad (50)$$

the subscript  $Z$  denotes partial differentiation with respect to  $Z$ , and the last equation in (49) is formed from a combination of the last two in (19); we have put  $R = 0$  on the basis that it is small. The boundary conditions for (49) are

$$\begin{aligned} \alpha = 0, \quad c = c_0, \quad \phi = \phi_0, \quad p = 0 & \quad \text{on } Z = 1, \\ c = c_E, \quad u_n = 0 & \quad \text{on } Z = 0. \end{aligned} \quad (51)$$

In principle, the upper and lower boundaries are free boundaries, but we will ignore that complication in our discussion.

Although the equations (49) are coupled, we think of the first and third as determining  $\mathbf{u}$  and  $p$ , the second as determining  $\alpha$ , the fourth as determining  $\phi$  and the fifth as determining  $c$ . The essence of the instability discussed above lies in the porosity equation for  $\phi$ , and specifically

$$c\phi_t = -(1-\alpha)\mathbf{u} \cdot \nabla c + \dots = (1-\alpha)(\nabla p \cdot \nabla c)\Pi(\phi) + \dots, \quad (52)$$

which promotes instability because  $\Pi'(\phi) > 0$ .

A model very similar to this has been studied by [Chiareli and Worster \(1995\)](#). Their concern was a possible instability in a mush formed from an alloy when a volume change took place. Their model was essentially equivalent to (49), except that they had  $\alpha = 0$ , and the rôle of our parameter  $\sigma$  is played by the term  $1 - r_{CW}$  in the Chiareli and Worster model, where  $r_{CW} = \rho_s/\rho_l$  was the density ratio between the phases. They found that the basic one-dimensional state was stable if  $r_{CW} > 1$  (shrinking on solidification, corresponding in our model to  $\sigma < 0$ ), but could be unstable for  $r_{CW} < 1$  (expansion on solidification, corresponding to  $\sigma > 0$ ) for sufficiently large values of the stability parameter

$$\mathcal{P} = \frac{\phi\Pi'(\phi)}{\Pi(\phi)}, \quad (53)$$

which we may, for example, take at the reference value  $\phi = \phi_0$ . The critical value of  $\mathcal{P}$  for instability was a decreasing function of  $\sigma$ , but still very large for  $\sigma < 1$ ; however, their results suggest that in practice, instability may realistically occur in our model for  $\mathcal{P} \sim 1$  if  $\sigma > 1$ . The following considerations suggest that this may be true. Note that, here, we do not conduct a complete stability analysis, since our present purpose is to proceed to the computation of pipes (vesicular cylinders) themselves.

More precisely, figure 5 shows the stability curve of Chiareli and Worster, together with an algebraic fit, described below. The question of interest is whether the decrease in  $\mathcal{P}$  is sufficient to make  $\mathcal{P} \sim O(1)$  for our value of  $\sigma \sim 2.7$ .

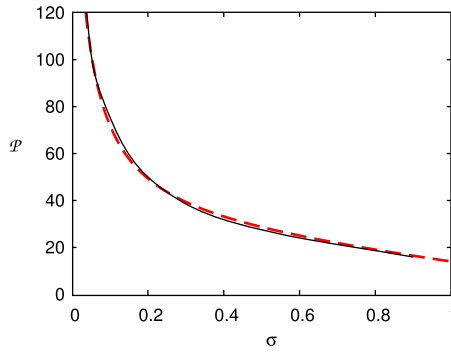


Figure 5. The critical value of the stability parameter  $\mathcal{P}$  as a function of  $\sigma$ , redrawn from Chiareli and Worster (1995), figure 5a. Also shown is a fitted dashed curve (red online), which is the curve that extends to  $\sigma = 1$ , and given by (60).

To assess this, we linearise (49), and will ignore variations in  $\alpha$ . First, we note that the basic state described by the steady travelling wave in section 2.5 has

$$\phi' > 0, \quad p' < 0, \quad c' < 0, \quad (54)$$

where the primes denote derivatives with respect to  $Z$ , not  $\xi$ . The linearised equations are denoting the steady state variables ( $\mathbf{u} = (u, w)$ ,  $\phi, c, p$ ) with small letters and the perturbed quantities with capitals,

$$\begin{aligned} U_x + W_Z &= \sigma(V\Phi_Z - \Phi_t), \\ U &= -\Pi P_x, \quad W = -\Pi P_Z - \Pi' p' \Phi, \\ (1 - \alpha)[\phi(C_t - VC_Z) + c'W + wC_Z] &= c(\Phi_t - V\Phi_Z) + V\phi' C, \\ (1 - \phi)(C_t - VC_Z) + Vc'\Phi &= \nabla^2 C + (c + St)(\Phi_t - V\Phi_Z) - V\phi' C, \end{aligned} \quad (55)$$

where  $\Pi' = \Pi'(\phi)$ . Now, we take all the unperturbed quantities  $w, c'$ , etc. to be constant (we do not expect this to be a significant quantitative assumption), and we look for normal mode solutions  $\propto \exp[\lambda t + ik_1 x + ik_3 z]$ . Some algebra then leads us to a quadratic equation for  $\lambda$ , and if we assume, as did Chiareli and Worster, that instability occurs directly, when  $\lambda = 0$ , we are then led to an expression for the corresponding critical value of  $\Pi'$ , which takes the form

$$(1 - \alpha)|c'| \left[ \frac{\Pi' w}{\Pi} + \frac{\sigma V k_3^2}{k^2} \right] = F, \quad (56)$$

where

$$\begin{aligned} F &= \frac{V[\phi' V F_1 + k_3^2(1 - \alpha)(w - \phi V) F_2]}{(k^2 + V\phi')^2 + k_3^2 V^2(1 - \phi)^2}, \\ F_1 &= |c'| (k^2 + V\phi') + k_3^2 V(1 - \phi)(c + St), \\ F_2 &= (c + St)(k^2 + V\phi') - |c'| V(1 - \phi), \end{aligned} \quad (57)$$

and

$$k^2 = k_1^2 + k_3^2. \quad (58)$$

This is the real part of the quadratic equation with  $\lambda = 0$ ; the imaginary part determines the corresponding horizontal wavenumber  $k_1$ , while the boundary conditions provide the vertical

wavenumber  $k_3$ . Solutions  $C \propto \sin \pi Z$ , for example, would imply  $k_3 = \pi$ , which we suppose is typical, but we do not carry out the full calculation.

We are particularly interested in the dependence of  $\mathcal{P}$  on  $\sigma$ . We use (42) and (53) to write (56) in the form

$$\sigma \left[ \left( \frac{X_E - 1}{X_E + \sigma(X_E - 1)} \right) \mathcal{P} + \frac{k_3^2}{k^2} \right] = \frac{F}{(1 - \alpha)|c'|V}. \quad (59)$$

There is little further we can do with this. Clearly  $F$  depends on  $\sigma$ , since also  $\phi$ ,  $c$  and  $k_1$  will. The fit used in figure 5 takes

$$\mathcal{P} = \frac{6.2}{\sigma + 0.03} + 26 - 18\sigma, \quad (60)$$

which is essentially equivalent to choosing a quadratic for  $F$ , and we suppose the large coefficients are due to the presence of  $k_3^2 \sim 10$ . While there is nothing optimal about this fit, it is noticeable in seeking it that the data seem to demand a linearly decreasing trend at larger  $\sigma$ ; and for the particular choice in figure 5,  $\mathcal{P} = 0$  when  $\sigma = 1.65$ . These considerations suggest to us that the steady state is likely to be unstable for values of  $\mathcal{P} \sim O(1)$  when  $\sigma = 2.7$ , and this prompts us to seek numerical solutions which represent channelled flow.

#### 4. Numerical results

In order to solve the problem numerically, we adopt a modified form of (49):

$$\begin{aligned} \nabla \cdot \mathbf{u} &= \sigma(V\phi_Z - \phi_t), \\ (\phi\alpha)_t - V(\phi\alpha)_Z &= \nabla \cdot ((1 - \alpha)\mathbf{u}) + \varepsilon \nabla^2 \alpha, \\ \mathbf{u} &= -\Pi(\phi)\nabla p + Ra\mathbf{k}, \\ (1 - \alpha)(\phi c_t - V\phi c_Z + \mathbf{u} \cdot \nabla c) + c(\phi_t - V\phi_Z) &= 0, \\ (1 - \alpha\phi)(c_t - Vc_Z) + (1 - \alpha)\mathbf{u} \cdot \nabla c &= \nabla^2 c + St(\phi_t - V\phi_Z), \end{aligned} \quad (61)$$

and we use the (dimensionless) Carman–Kozeny law

$$\Pi = \frac{\phi^3}{(1 - \phi)^2}. \quad (62)$$

The boundary conditions for (61) are initially taken to be

$$\begin{aligned} \alpha = 0, \quad c = c_0, \quad \phi = \phi_0, \quad p = 0 \quad \text{on} \quad Z = 1, \\ \alpha_Z = 0, \quad c = c_E, \quad u_n = 0 \quad \text{on} \quad Z = 0. \end{aligned} \quad (63)$$

These equations are the same as those in (49), with the exception of the term  $\propto \varepsilon$  in (61)<sub>2</sub>. The point is that we can only prescribe  $\alpha = 0$  on the top surface if  $u_n < \phi V_n$  there (cf. (21)). This would be numerically awkward, but is alleviated by including the diffusive term. If  $\varepsilon \ll 1$ , then the actual equation for  $\alpha$  provides the sub-characteristics for (61)<sub>2</sub>, and the solutions for the two systems will be the same, except for a thin boundary layer at the top surface where  $u_n > \phi V_n$ . The prescription of zero gradient at the base precludes the formation of a serious boundary layer there. We do not show the resulting simulations (which use the parameters in figure 4, and additionally  $\varepsilon = 0.001$ ), because the steady solutions in figure 4 exactly overlay the numerically computed solutions of (61).

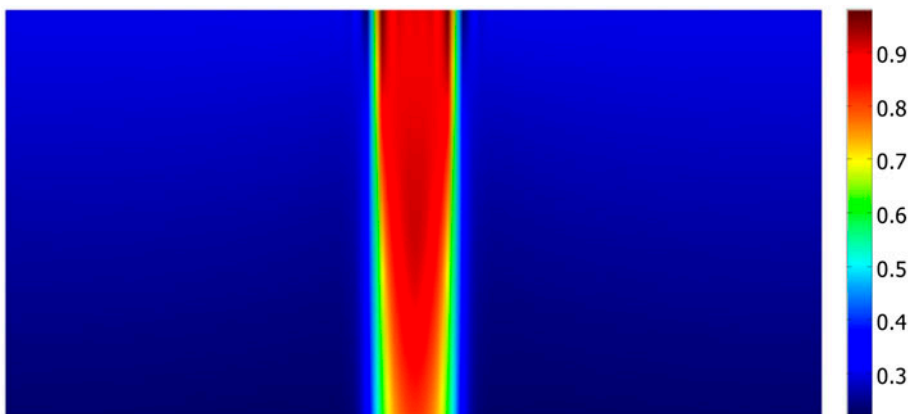


Figure 6. Simulation of a steady channel by solving (61) and (63), except that  $\phi$  is given at the surface by (64). The colour scale gives the value of the porosity  $\phi$ . As described in the text, the domain is of dimensionless height 1 ( $0 < Z < 1$ ) and width 2 ( $-1 < x < 1$ ), while the elevated porosity at the surface is applied over a width 0.1 ( $-0.05 < x < 0.05$ ). The parameter values are as in figure 4, and additionally  $a = 0.05$ ,  $\phi_v = 0.9$   $\varepsilon = 0.001$ .

Disappointingly, no instability or channel-like solutions are in evidence. The issue is clouded, however, by the observation that if vesicular channels were to form, then there is upflow in them relative to the upper surface, and it is no longer appropriate to prescribe  $\phi = \phi_0$  at the surface where a channel exists. More precisely, if channels exist in which  $\phi > \phi_0$ , then in fact the mush surface is not flat, since it bends downwards along the channel walls. The implication is that the prescription of constant  $\phi$  at the top surface precludes the formation of channels.

In a second simulation, we prescribe a top hat profile for  $\phi$  at the surface:

$$\begin{aligned} \phi &= \phi_v & \text{on } Z = 1, & & |x| < a, \\ \phi &= \phi_0 & \text{on } Z = 1, & & a < |x| < 1, \end{aligned} \quad (64)$$

and we choose  $a$  to be small and  $\phi_v$  close to one. The following argument suggests that vesicular channels may form in this case. If they do not, then  $\phi$  must decrease rapidly below the surface,† presumably attaining the steady solutions of figure 4. In that case  $\dot{\phi} = \phi_t - V\phi_Z$  is large and negative, so that (49)<sub>1</sub> implies  $\nabla \cdot \mathbf{u}$  is large and positive. It seems unlikely that this will be taken up by  $u_x$ , so that we would take (in a steady state)

$$w_Z \approx \sigma V \phi_Z, \quad (65)$$

so that the excess upwards velocity at the hole is approximately  $\sigma V(1 - \phi_0)$ . Using (42), it follows after some algebra that  $w|_{Z=1} > V$  at the hole if

$$\sigma > \frac{[(1 - \phi_0)^2 + 4(1 - \phi_0)X_E(X_E - 1)]^{1/2} - (1 - \phi_0)}{2(X_E - 1)(1 - \phi_0)}, \quad (66)$$

and this is our approximate channel-forming criterion.

†Alternatively, the change in  $\phi$  could radiate diffusely away from the surface source at  $x \approx 0$ . In this case,  $\nabla \cdot \mathbf{u} > 0$  over a broad region, and presumably the fluid is sucked towards the central “hole”, where we would expect the exit velocity to be large and ill-posedness to ensue.

Figure 6 shows the result of a simulation in which the top hat profile in (64) has been applied. For the values used in the figure, the channel-forming criterion (66) is  $\sigma > 1.23$ , so that we expect a channel to form, and indeed this is what the figure shows. Indeed, this simulation supports our theoretical discussion above. The calculations were done using the finite element-based software, Comsol Multiphysics, and are limited to a steady state calculation. All field equations were discretised using second-order quadrilateral elements on a mapped uniform mesh having 2500 ( $50 \times 50$ ) elements, corresponding to around 41,300 degrees of freedom.

## 5. Conclusions

We have provided a consistent, physically based explanation for vesicular cylinders in crystallising basaltic lavas. Our explanation is based on the apparent resemblance of these vertical cylinders to similar channels or pipes which form in solidifying binary alloys, and our initial efforts to explain them hypothesised that a similar explanation would suffice. Specifically, release of light fluid in crystallising mushes of, for example, ammonium chloride drives porous medium convection within the mush. If this is sufficiently vigorous (if the upwards fluid velocity exceeds the solidification rate), then channels form and are observable in the cast because of the colour difference associated with late-stage crystallisation. In this way, “freckles” are formed in, for example, lead-tin alloys.

In the present situation, we also have a crystallising mush, in which the buoyancy source is due to gas bubble formation, and the mathematical model we develop is similar to (but more general than) the alloy solidification model, but the effective Rayleigh number we determined is more than two orders of magnitude too low for convection to occur in the basalt lava flow mush. However, the model was sufficiently rich that convection was not necessary; all that the channel-forming mechanism requires is a differential fluid velocity, and this is afforded by the expansion parameter  $\sigma$ . Proceeding on this basis, we identified a plausible instability mechanism, which is that outlined in 3: increased local porosity causes increased upwards fluid flow, which brings more silicic melt up. The higher up liquid, being more silicic, has a lower liquidus temperature, which promotes, if not melt-back, at least a decreased rate of crystallisation, and thus a relative further growth of porosity. We then showed, in a rough stability analysis, that this positive feedback mechanism does provide for the growth of vertically oriented patterns.

Finally, we provided numerical computations which show that there are steady solutions in which cylinders are formed, and we thus consider that this model provides a viable explanation for vesicular cylinder formation in inflated basalt lava flows. Similar processes could aid segregation of evolved melts from crystallising volatile-saturated magma intrusions. Just as in the simpler models describing alloy solidification, however, the story is by no means over. Our theory has adopted numerous simplifications in order to approach our goal of demonstrating the viability of channel formation, and in the context of freckle formation in alloy solidification, the work of Worster and his co-workers over the last 30 years shows that a thorough analysis of the problem requires a good deal more investigation than is presented here (e.g. Schulze and Worster 1999, 2005, Chung and Worster 2002). The principal limitation in our discussion of the model is the short-circuiting of the complexity associated with the upper free boundary condition. In addition, although our numerical simulation in figure 6 is suggestive of channel formation, we have no independent way to compare the computed channel width with observations such as those in figure 1, since in figure 6, we simply prescribe the channel

width. In future work, it will be essential to include a description of the upper surface as a free surface, something which is not attempted in the present paper.

From a theoretical perspective, our study suggests that convection is not a necessary prerequisite for channel formation, so long as density change-induced fluid (silicate melt with suspended bubbles) velocities are sufficiently rapid. The geological record indicates that vesicular cylinders are common in inflated pahoehoe lava flows, and do not form in other types of basalt lava flows such as 'a'a, which is characterised by shear-induced tearing (e.g. Goff 1996, Self *et al.* 1998). The association with inflation indicates that vesicular cylinders form in lava flows emplaced with relatively low crystallinity and on nearly flat ground; however, the specific conditions for their formation have not been well constrained empirically or theoretically. In the context of our proposed model, there are a number of factors that could affect the presence or absence of vesicular cylinders in an inflated lava flow, such as the initial magma bubble and crystal content or the shape and size distribution of crystals, which in turn would affect both the mush permeability and the threshold crystallinity at which the crystal network in a magma mush acts as a porous medium. A key component of our channel-forming model is the isolation of the bubbles, and the vesicular cylinders would not grow if the vesicularity of the mush was so high that H<sub>2</sub>O exsolution could be accommodated by gas flow through a connected gas pathway rather than pushing liquid melt up through the crystal mush. Although cylinders and other segregation features in lava flows are not in and of themselves important, these features, found around the world in readily accessible outcrops, provide insights into the role of bubbles in the segregation of crystalline magmas which may be important for understanding the evolution of magma reservoirs beneath volcanoes and the triggering of volcanic eruptions.

## Acknowledgements

A. C. F. and M. V. acknowledge the support of the Mathematics Applications Consortium for Science and Industry ([www.macsi.ul.ie](http://www.macsi.ul.ie)) funded by the Science Foundation Ireland grant 12/1A/1683. A. C. R. acknowledges support from a Royal Society URF and Natural Environment Research Council (UK) grant NE/J021210/1. We also thank Mark McGuinness for discussions and assistance, and Paul Lyle for helpful suggestions for finding field examples in Northern Ireland.

## References

- Anderson, A.T., Swihart, G.H., Artioli, G. and Geiger, C.A., Segregation vesicles, gas filter-pressing, and igneous differentiation. *J. Geol.* 1984, **92**, 55–72.
- Caroff, M., Maury, R.C., Cotten, J. and Clément, J.-P., Segregation structures in vapor-differentiated basaltic flows. *Bull. Volcanol.* 2000, **62**, 171–187.
- Cashman, K.V. and Kauahikaua, J.P., Reevaluation of vesicle distributions in basaltic lava flows. *Geology* 1997, **25**, 419–422.
- Chiareli, A.O.P. and Worster, M.G., Flow focusing instability in a solidifying mushy layer. *J. Fluid Mech.* 1995, **297**, 293–305.
- Chung, C.A. and Worster, M.G., Steady-state chimneys in a mushy layer. *J. Fluid Mech.* 2002, **455**, 387–411.
- Costa, A., Blake, S. and Self, S., Segregation processes in vesiculating crystallizing magmas. *J. Volcanol. Geotherm. Res.* 2006, **153**, 287–300.
- Dowden, J., Kapadia, P., Brown, G. and Rymer, H., Dynamics of a geyser eruption. *J. Geophys. Res.* 1991, **96**(B11), 18059–18071.
- Flemings, M.C., *Solidification Processing*, 1974 (McGraw-Hill: New York).
- Fowler, A.C., *Mathematical Geoscience*, 2011 (Springer-Verlag: London).
- Fowler, A.C., Kopteva, N. and Oakley, C., The formation of river channels. *SIAM J. Appl. Math.* 2007, **67**, 1016–1040.

- Goff, F., Vesicle cylinders in vapor-differentiated basalt flows. Ph.D. Thesis, University of California, Santa Cruz, 1977.
- Goff, F., Vesicle cylinders in vapor-differentiated basalt flows. *J. Volcanol. Geotherm. Res.* 1996, **71**, 167–185.
- Groves, C.G. and Howard, A.D., Minimum hydrochemical conditions allowing limestone cave development. *Water Resour. Res.* 1994, **30**, 607–615.
- Hartley, M.E. and Thordarson, T., Melt segregations in a Columbia River Basalt lava flow: A possible mechanism for the formation of highly evolved mafic magmas. *Lithos* 2009, **112**, 434–446.
- Hersum, T., Hilpert, M. and Marsh, B., Permeability and melt flow in simulated and natural partially molten basaltic magmas. *Earth Planet. Sci. Lett.* 2005, **237**, 798–8148.
- Hewitt, I.J. and Fowler, A.C., Melt channelization in ascending mantle. *J. Geophys. Res.* 2009, **114**, B06210.
- Hon, K., Kauahikaua, J., Denlinger, R. and Mackay, K., Emplacement and inflation of pahoehoe sheet flows: Observations and measurements of active lava flows on Kilauea Volcano. *Hawaii. Geol. Soc. Amer. Bull.* 1994, **106**, 351–370.
- Kelemen, P.B., Hirth, G., Shimizu, N., Spiegelman, M. and Dick, H.J.B., A review of melt migration processes in the adiabatically upwelling mantle beneath oceanic spreading ridges. *Philos. Trans. R. Soc. Lond.* 1997, **A355**, 283–318.
- Kontak, D.J. and Dostal, J., The late-stage crystallization history of the Jurassic North Mountain Basalt, Nova Scotia, Canada. II. Nature and origin of segregation pipes. *Canad. Mineral.* 2010, **48**, 1533–1568.
- Kuritani, T., Yoshida, T. and Nagahashi, Y., Internal differentiation of Kutsugata lava flow from Rishiri Volcano, Japan: Processes and timescales of segregation structures' formation flows. *J. Volcanol. Geotherm. Res.* 2010, **195**, 57–68.
- Lapwood, E.R., Convection of a fluid in a porous medium. *Proc. Camb. Phil. Soc.* 1948, **44**, 508–521.
- Lister, J.R. and Kerr, R.C., The effect of geometry on the gravitational instability of a buoyant region of viscous fluid. *J. Fluid Mech.* 1989, **202**, 577–594.
- Loewenherz, D.S., Stability and the initiation of channelized surface drainage: A reassessment of the short wavelength limit. *J. Geophys. Res.* 1991, **96**, 8453–8464.
- Loewenherz-Lawrence, D.S., Hydrodynamic description for advective sediment transport processes and rill initiation. *Water Resour. Res.* 1994, **30**, 3203–3212.
- Manga, M. and Stone, H.A., Interactions between bubbles in magmas and lavas: effects of bubble deformation. *J. Volcanol. Geotherm. Res.* 1994, **63**, 267–279.
- Philpotts, A.R. and Carroll, M., Physical properties of partly melted tholeiitic basalt. *Geology* 1996, **24**, 1029–1032.
- Rogan, W., Blake, S. and Smith, I., In situ chemical fractionation in thin basaltic lava flows: Examples from the Auckland volcanic field, New Zealand, and a general physical model. *J. Volcanol. Geotherm. Res.* 1996, **74**, 89–99.
- Röthlisberger, H., Water pressure in intra- and subglacial channels. *J. Glaciol.* 1972, **11**, 177–203.
- Schulze, T.P. and Worster, M.G., Weak convection, liquid inclusions and the formation of chimneys in mushy layers. *J. Fluid Mech.* 1999, **388**, 197–215.
- Schulze, T.P. and Worster, M.G., A time-dependent formulation of the mushy-zone free-boundary problem. *J. Fluid Mech.* 2005, **541**, 193–202.
- Self, S., Keszthelyi, L. and Thordarson, Th., The importance of pāhoehoe. *Ann. Rev. Earth Planet. Sci.* 1998, **26**, 81–110.
- Sigmarsson, O., Thordarson, T. and Jakobsson, S.P., Segregations in Surtsey lavas (Iceland) reveal extreme magma differentiation during late stage flow emplacement. *Studies in Volcanology: The Legacy of George Walker, Spec. Publ. IAVCEI* 2009, **2**, 85–104.
- Smith, T.R. and Bretherton, F.P., Stability and the conservation of mass in drainage basin evolution. *Water Resour. Res.* 1972, **8**, 1506–1529.
- Stephenson, P.J., Zhang, M. and Spry, M., Fractionation modelling of segregations in the Toomba Basalt, north Queensland. *Austral. J. Earth Sci.* 2000, **47**, 291–300.
- Tait, S., Jahrling, K. and Jaupart, C., The planform of compositional convection and chimney formation in a mushy layer. *Nature* 1992, **359**, 406–408.
- Tait, S. and Jaupart, C., Compositional convection in a reactive crystalline mush and melt differentiation. *J. Geophys. Res.* 1992, **97**, 6735–6756.
- Wettlaufer, J.S., Worster, M.G. and Huppert, H.E., Natural convection during solidification of an alloy from above with application to the evolution of sea ice. *J. Fluid Mech.* 1997, **344**, 291–316.
- Worster M.G., Solidification of an alloy from a cooled boundary. *J. Fluid Mech.* 1986, **167**, 481–501.
- Worster, M.G., Convection in mushy layers. *Ann. Rev. Fluid Mech.* 1997, **29**, 91–121.

## Appendix

The following two tables (Latin and Latin/Greek, respectively) list all the mathematical symbols used in the text, and the (nearest) equation or figure where they are introduced.

Table A.1. Mathematical symbols (Latin).

Symbol	Meaning	Location
$a$	Dimensionless channel width	(64)
$b$	Mush–solid interface	Figure 3
$c$	Magma composition	Figure 2
$c_E$	Eutectic composition	Figure 2
$c_{H_2O}$	Water saturation	(5)
$c_l$	Liquid composition	Figure 2
$c_p$	Average specific heat	(9)
$c_{pg}$	Gas specific heat	(10)
$c_{pl}$	Liquid specific heat	(10)
$c_{ps}$	Solid specific heat	(9)
$c_s$	Crystal composition	Figure 2
$C$	Perturbation of $c$	(55)
$d$	Magma depth	(14)
$D$	Crystal size	Before (49)
$F, F_1, F_2$	Stability coefficients	(57)
$g$	Gravity	(4)
$h$	Mush–liquid interface	Figure 3
$\hat{\mathbf{k}}$	Unit vertical vector	(4)
$K$	Permeability	(4)
$K_0$	Permeability scale	(16)
$k$	Vertical wave number	(58)
$k_g$	Wavenumber	(10)
$k_l$	Liquid thermal conductivity	(10)
$k_s$	Solid thermal conductivity	(10)
$k_T$	Thermal conductivity	(9)
$k_1$	Horizontal wave number	After (55)
$k_3$	Vertical wave number	After (55)
$L_c$	Latent heat of crystallisation	(9)
$L_v$	Latent heat of exsolution	(9)
$m_c$	Rate of crystallisation	(1)
$m_L$	Liquidus slope	(11)
$m_v$	Rate of exsolution	(6)
$m_s$	Surface source term	(7)
$p$	Melt pressure	(4)
$P$	Perturbation of $p$	(55)
$\mathcal{P}$	Permeability sensitivity	(53)
$r$	Solid–liquid density difference parameter	(18)
$r_{CW}$	Chiareli–Worster parameter	Before (53)
$R$	Effective Rayleigh number	(18)
$St$	Stefan number	(18)
$S_v$	Vapour Stefan number	(18)

Table A.2. Mathematical symbols (Latin), continued, and Greek.

Symbol	Meaning	Location
$t$	Time	(1)
$T$	Temperature	Figure 2
$T_E$	Eutectic temperature	Figure 2
$T_L$	Liquidus temperature	(11)
$T_0$	Pure liquid melting temperature	Figure 2
$\mathbf{u}$	Fluid flux	(3)
$u_n$	Normal component of fluid flux	(21)
$U$	Horizontal component of $\mathbf{u}$	(55)
$V$	Travelling wave speed	(34)
$\mathbf{V}$	Surface velocity	(29)
$V_n$	Normal component of surface velocity	(21)
$w$	Vertical component of $\mathbf{u}$	(31)
$W$	Perturbation of $w$	(55)
$X$	Dimensionless concentration	(37)
$X_E$	Dimensionless eutectic concentration	(38)
$z$	Vertical spatial coordinate	Figure 3
$Z$	Travelling wave coordinate	(50)
$\alpha$	Gas volume fraction	Figure 3
$\beta$	Adiabatic heating parameter	(18)
$\gamma_+$	Upper dimensionless heat flux	(22)
$\gamma_-$	Lower dimensionless heat flux	(26)
$\delta$	Gas–liquid density ratio	(18)
$\eta_l$	Melt viscosity	(4)
$\kappa_T$	Thermal diffusivity	(15)
$\lambda$	Growth rate	After (55)
$\Lambda$	Partition coefficient	(12)
$\xi$	Travelling wave variable	(34)
$\xi_b$	Dimensionless mush depth	(34)
$\Pi$	Dimensionless permeability	(16)
$\rho$	Pore fluid density	(2)
$\rho_s$	Crystal density	(1)
$\rho_l$	Melt density	(2)
$\rho_g$	Water vapour density	(2)
$\sigma$	Dissolved to exsolved vapour density ratio	(18)
$\phi$	Mush porosity	Figure 3
$\phi_0$	Mush surface porosity	Figure 3
$\phi_b$	Basal porosity	(40)
$\phi_v$	Pipe surface porosity	(64)
$\Phi$	Perturbation of $\phi$	(55)